Environmental Pollution 185 (2014) 213–218

Contents lists available at ScienceDirect

Environmental Pollution

journal homepage: www.elsevier.com/locate/envpol

Sorption of phenanthrene and benzene on differently structural kerogen: Important role of micropore-filling

Yulong Zhang [a], Xiaoxuan Ma [a,b], Yong Ran [a,*]

[a] State Key Laboratory of Organic Geochemistry, Guangzhou Institute of Geochemistry, Chinese Academy of Sciences, 511 Kehuajie, Tianhe District, Guangzhou 510640, China
[b] School of Resources and Environment Engineering, Shandong University of Technology, Zibo 255049, China

ARTICLE INFO

Article history:
Received 1 August 2013
Received in revised form
24 October 2013
Accepted 30 October 2013

Keywords:
Kerogen
Benzene
Phenanthrene
Sorption
Hole-filling

ABSTRACT

Shale was thermally treated to obtain a series of kerogen with varied maturation. Their chemical, structural and porous properties were related to the sorption and/or desorption behaviors of phenanthrene and benzene. As the treatment temperature increases, aliphatic and carbonyl carbon of the kerogen samples decrease, while their aromaticity and maturation increase. Meanwhile, the isothermal nonlinearity of phenanthrene and benzene increases whereas the sorption capacity and micropore adsorption volumes ($V_{o,d}$) initially increase and then decrease. The $V_{o,d}$ of benzene is significantly correlated with, but higher than that of phenanthrene, suggesting similar micropore filling mechanism and molecular sieve effect. The benzene desorption exhibits hysteresis, which is related to the pore deformation of the kerogen and the entrapment of solute in the kerogen matrix. The $V_{o,d}$ of phenanthrene and benzene on the kerogen samples accounts for 23–46% and 36–65% of the maximum sorption volumes, respectively, displaying the importance of the micropore filling.

1. Introduction

Sorption of hydrophobic organic chemicals (HOCs) by natural organic matter (NOM) in water, soils, and sediments controls their bioavailability, risk, and fate (Chefetz and Xing, 2009; Luthy et al., 1997; Pignatello and Xing, 1996). Some studies have indicated that porosity and surface properties of NOM play a significant role in controlling the sorption (Kleineidam et al., 2002; Pignatello, 2012; Ran et al., 2002, 2004, 2013).

The dual-sorption model has characterized NOM as two domains containing absorption (partitioning) and adsorption (micropore-filling) phases (Weber and Huang, 1996; Weber and Young, 1997; Xing and Pignatello, 1997; Ran et al., 2003). Kerogen is a form of NOM that has undergone geochemical diagenesis. Kerogen dominantly consists of flexible aliphatic moieties and rigid aromatic moieties, which consist of partitioning phase and pore-filling phase, respectively (Cornelissen et al., 2005). In addition, the surface and porosity properties of kerogen significantly change during thermal maturation from 250 °C to 500 °C (Yang et al., 2009). Thus, a series of differently matured kerogen could be ideal materials to elucidate the sorption mechanism of different domains and the importance of microporosity of NOM in the sorption.

The microporosity and surface characteristics of NOM are important for understanding the sorption process of HOCs. The porosity of NOM has been extensively evaluated by N_2 adsorption technique (Kwon and Pignatello, 2005; Ravikovitch et al., 2005; Xing and Pignatello, 1997). However, this technique has been found to underestimate the contribution of soil/sediment NOM microporosity (Ran et al., 2013). The specific surface areas of NOM based on CO_2 adsorption differ significantly from those using N_2 adsorption, primarily due to the molecular sieving phenomenon (De Jonge and Mittelmeijer-Hazeleger, 1996; Xing and Pignatello, 1997). Some internal pores of organic matrices can not be approached by N_2 (Gan et al., 1972; Larsen et al., 1995). Carbon dioxide at 273 K and benzene at 295 K have been used as alternative gases for probing the surface properties of carbonaceous materials (Corley et al., 1996; De Jonge and Mittelmeijer-Hazeleger, 1996; Kwon and Pignatello, 2005; Ravikovitch et al., 2005; Xing and Pignatello, 1997). They are not affected by molecular sieving, resulting in a surface area of 1–2 orders of magnitude higher than that using N_2 (De Jonge and Mittelmeijer-Hazeleger, 1996; Ran et al., 2013; Xing and Pignatello, 1997). Much of the benzene- or CO_2-derived surface area is tightly associated with internal NOM matrices (Ran et al., 2013). The majority of the surface area of NOM is formed by micropores and submicropores (0.3–0.5 nm) (Braida

* Corresponding author.
E-mail address: yran@gig.ac.cn (Y. Ran).

0269-7491/$ – see front matter © 2013 Elsevier Ltd. All rights reserved.
http://dx.doi.org/10.1016/j.envpol.2013.10.039

et al., 2003; Li and Werth, 2001). Pore-filling of HOCs can account for 45–98% of total sorption by peat and soil (Ran et al., 2004; Xing et al., 1996; Xing and Pignatello, 1997). Although these surveys provide valuable insights into the relationship between porosity and sorption, the importance of the microporosity and surface area of NOM on the sorption of HOCs remains poorly understood.

In the present study, a kerogen sample was thermally simulated to become mature, causing a series of changes in composition, structure and microporosity. The original and matured kerogen samples were used as sorbents and phenanthrene was used as a sorbate to obtain the aqueous sorption data. Benzene is a basic unit of phenanthrene. It has been found that benzene and phenanthrene can be sorbed to similar micropores of NOM (Sun et al., 2013). Thus, gaseous benzene could be suitable to characterizing microporosity of sorbents. Therefore, we used benzene as a sorbate to model the gas sorption on kerogen. The importance of micropores for the sorption of HOCs by glassy NOM was investigated.

2. Materials and methods

2.1. Sample collection and treatment

A shale sample was collected from Maoming city, southwest of Guangdong Province, China. It contained type II kerogen derived from lacustrine sedimentation (Ran et al., 2007). Prior to storage in an argon-filled glass container, the sample was ground to pass through a sieve (200 mesh). Six subsamples of about 5 g were mixed with deionized water of 2 ml and were separately sealed in steel ampoules. The ampoules were heated in a muffle furnace with a temperature sequence (20 °C/min from 25 °C to 200 °C, followed by 2 °C/min from 200 °C to 500 °C). This mimicking diagenesis procedure was detailed previously (Yang et al., 2009). After thermal treatment, the matured and original kerogen samples were ground again. Carbonates were removed with 1 N HCl, followed by a de-ashing treatment upon a mixed acid solution of HCl and HF for 5 d. The residual acid was rinsed off three times, and then the residual solid was dried in an oven. Thereafter, a solvent mixture of methanol: acetone: benzene (1:2.5:2.5, v:v:v) was applied to remove some extractable components via a Soxhlet equipment. The treated samples were dried under vacuum for 10 days. The six matured kerogen and their parental kerogen were finely ground.

2.2. Characterization of the kerogen samples

The elemental compositions (C, H, N, and O) were measured using an Elementar Vario EL III. The solid-state ^{13}C nuclear magnetic resonance (^{13}C NMR) spectra were determined on a Bruker DRX-400 NMR spectrometer. The sample was loaded in a 4-mm diameter ZrO_2 rotor. The NMR program was as follows: ^{13}C frequency of 100.63 MHz, magic-angle-spinning rate of 6.0 kHz, recycle time of 1.2 s, and contact time of 1.2 ms. Besides, the 500 °C-matured kerogen was also measured with a total sideband suppression (TOSS) technique. A Perkin–Elmer 1725 X infrared spectrophotometer was used to generate the Fourier transformed infrared (FTIR) spectra. The vitrinite reflectance (R_o) was measured using Leitz MPV-3 and was indicative of the rigidity of kerogen (Ran et al., 2002). The specific surface areas were determined using the N_2 adsorption/desorption data at an ASAP-2010 (Micromeritics, Norcorss, GA) instrument. The analysis procedure was described previously (Ran et al., 2013). The physiochemical properties of the kerogen samples are listed in Tables 1 and 2.

2.3. Phenanthrene sorption experiments

All sorption isotherms of phenanthrene were obtained using a batch equilibration technique in 50 mL glass ampoules at room temperature. Background solution was simulated with 0.005 M $CaCl_2$ and 0.1 g/L NaN_3. Eleven initial phenanthrene concentrations varying from 5 to 1000 μg/L were used for a single isotherm. Solid-solution contact times of 42 d were used to reach apparent sorption equilibrium. After the equilibrium, the sorbent-solution mixture was settled, allowing solid particles to precipitate. The supernatant of 1.5 mL was mixed with the weighted methanol, followed by an analysis using a reverse phase HPLC (ODS, 250 × 2.0 mm, Phenomenex) with ultraviolet and fluorescence detectors. The sorbed phenanthrene on the sorbents was calculated by mass balance.

The sorption data were fitted to the Freundlich model:

$$Q_e = K_F C_e^n \quad (1)$$

where Q_e is the solid-phase concentration (μg/g), and C_e is the liquid-phase equilibrium concentration (μg/L). K_F is the Freundlich sorption distribution coefficient [(μg/g)/(μg/L)^n], and n is the isotherm nonlinearity index. The modeling results and the fitting parameters are listed in Table 3.

Table 2
Carbon functional groups derived from ^{13}C NMR.

Sample	Aliphatic (0–93 ppm)	Aromatic (93–165 ppm)	Carbonyl (165–220 ppm)	f_a[a] (%)	f_b[b] (%)
RJ0	76.0	16.6	7.4	17.9	82.1
RJ1	74.0	20.3	5.6	21.6	78.5
RJ2	74.1	21.3	4.6	22.3	77.7
RJ3	50.8	49.2	/	49.2	50.8
RJ4	25.8	74.2	/	74.2	25.8
RJ5	10.0	90.0	/	90.0	10.0
RJ6	7.1	92.9	/	92.9	7.1
RJ6TOSS	8.4	91.6	/	91.6	8.4

[a] f_a represents aromaticity.
[b] f_b represents aliphaticity.

2.4. Benzene vapor adsorption and desorption

Gravimetric sorption measurements of benzene in the matured and original kerogen were carried on with an Intelligent Gravimetric Analyser. In each run, 70 mg sample was loaded. Prior to sorption experiment, the system was vacuumed for several times to remove gas initially sorbed on the samples. The sorption and desorption isotherms of benzene were obtained using the Freundlich model. The modeled parameters are shown in Table 4.

Based on the sorption isotherms, maximum sorption volumes (V_{max}) of benzene and phenanthrene were estimated when the equilibrium concentrations of benzene and phenanthrene are saturated in the gas and aqueous conditions. It should be noted that the calculated V_{max} includes both the partitioning and micropore-filling fractions. The calculation method was described in previous literatures (Ran et al., 2004, 2013).

2.5. Micropore volume modeling

The microvoid volume ($V_{o,d}$) of benzene and phenanthrene on the kerogen samples was obtained using the Dubinin-Radushkavich (DR) equation:

$$\mathrm{Log}V = \mathrm{log}V_{o,d} - D(\mathrm{log}p_o/p)^2 \quad (2)$$

$$\mathrm{Log}V = \mathrm{log}V_{o,d} - D(\epsilon_{sw}/V_s)^2 \quad (3)$$

where V and $V_{o,d}$ are the adsorbed and micropore volumes (μL/g) expressed as a liquid volume, assuming the liquid density of benzene is 0.879 g mL^{-1}, and D is a constant related to the energy of adsorption and the pore structure. ϵ_{sw} (cal/mol) is the effective adsorption potential of phenanthrene, and V_s is the molar volume (cm^3/mol) of phenanthrene.

Table 1
Physicochemical properties of the original and thermally matured kerogen samples.

Sample	Temp.[a] (°C)	C	N	H	O	O/C	H/C	Ash (%)	Yield	BET N_2 (m^2/g)	R_o (%)
RJ0	–	63.9	1.3	6.9	13.8	0.16	1.30	7.0	–	7.3	0.36
RJ1	250	68.3	2.9	5.9	13.0	0.14	1.00	2.1	40.3	4.0	0.48
RJ2	300	72.7	2.7	6.0	11.6	0.12	0.99	3.3	40.5	3.6	0.52
RJ3	350	68.7	3.3	5.7	9.5	0.10	0.99	5.6	40.5	5.0	0.76
RJ4	400	74.2	3.5	3.8	6.7	0.07	0.62	6.0	25.4	5.5	1.40
RJ5	450	77.0	4.0	4.0	5.2	0.05	0.62	4.7	25.4	10.0	2.10
RJ6	500	80.7	4.2	3.5	5.0	0.05	0.52	3.0	29.4	27.5	2.69

[a] Temperature of thermal simulation.

Table 3
Freundlich sorption parameters and single distribution coefficients for phenanthrene on the kerogen samples.

Sample	log K_F[a]	n	R^2	N[b]	K_{oc} (L/g)		
					$C_e = 0.005S_w$	$C_e = 0.05S_w$	$C_e = 0.5S_w$
RJ0	2.74(0.030)[c]	0.769(0.019)[c]	0.994	22	596	350	206
RJ1	2.80(0.046)	0.709(0.030)	0.984	22	578	296	151
RJ2	2.77(0.039)	0.753(0.025)	0.989	22	538	304	172
RJ3	2.71(0.038)	0.781(0.023)	0.988	21	566	342	207
RJ4	3.21(0.043)	0.628(0.033)	0.980	21	1201	510	217
RJ5	3.59(0.052)	0.522(0.050)	0.942	18	2341	779	259
RJ6	3.59(0.051)	0.399(0.041)	0.943	22	1834	460	115

[a] The unit of log K_F is $(\mu g/g)/(\mu g/L)^n$.
[b] The number of observation.
[c] Standard deviation.

3. Results and discussion

3.1. Physicochemical characteristics

The physical and chemical properties of the kerogen samples are listed in Tables 1 and 2. All the characteristics data well mirror the chemical, structural and porous changes of the kerogen during thermal alteration from 250 °C to 500 °C.

The ratios of H/C and O/C progressively decreased with the maturation trend of the kerogen (Table 1). It is worth noting that the former remained basically constant from RJ1 to RJ3, whereas the latter kept decreasing throughout the whole thermal process. This indicates that the decarboxylation predominated at the low temperature diagenesis stage (250 °C–350 °C) of the kerogen, which is consistent with the other geochemistry studies in which the mechanisms of such simulation procedure were well established (e.g. Durand, 1980; Yang et al., 2009). Significant decreases in ratios of O/C and H/C of the kerogen occurred above 400 °C. This is consistent with pyrolysis of plenty of aliphatic carbon in the kerogen. As dia- and catagenesis for the NOM fractions were developed, the atomic O/C and H/C ratios decreased, but the maturity index (R_o) increased.

The above dia- and catagenetic mechanisms of kerogen can be further supported by the data of solid-state ^{13}C NMR spectra (Fig. 1). The relative abundances of various functional groups via the integrations of peak areas are summarized in Table 2. Approximate band assignments are as follows: nonpolar alkyls (0–45 ppm), methoxy (45–63 ppm), O-alkyls (63–93 ppm), aromatics (93–148 ppm), aromatic C–O (148–165 ppm), carboxylic carbon (165–187 ppm), and ketones, quinones, and aldehydes (187–220 ppm). The relative peak intensity of the aliphatic C (0–45 ppm) decreased considerably from RJ3 to RJ4, while that of the aromatic C (93–165 ppm) increased significantly. This suggests a significant cracking of alkyl C from 350 °C to 400 °C. For the matured kerogen at 500 °C, aliphatic carbon is almost absent (Fig. 1B). In addition, it is noted that the signals of carbonyl C (187–220 ppm) and carbohydrate C (63–93 ppm) are present in the spectra of the highly-matured kerogens (RJ4-RJ6). However, such oxygen-containing functional groups are not present for the samples treated under 350 °C. The phenomena could be resulted from the ^{13}C NMR measurement procedure, rather than from the nature of the matured kerogen. When a total sideband suppression (TOSS) technique was applied to obtain a new ^{13}C NMR spectrum of RJ6 (Fig. 1B), no carbonyl and carbohydrate signals appear in the new spectrum, demonstrating that they are the side bands in the NMR measurement. Taking the side bands into account, integration of aromatic C for the highly matured kerogen (RJ4-RJ6) was deducted from their MAS-CP ^{13}C NMR results. The revised data are listed in Table 2. This above result suggests that ^{13}C NMR is a powerful approach for illustrating the carbon functional groups.

An additional evidence for the absence of carbonyl C in the highly-matured kerogen is provided by the FTIR spectra (Supplementary Data, Fig. S1), which shows no C=O stretching vibration of carbonyl C (1700 cm^{-1}) in the samples from RJ4 to RJ6. The decreasing C–H stretching vibration of methyl (2920 cm^{-1}) and methylene (2851 cm^{-1}) C from JR0 to JR7 is in accordance with the progressive removal of aliphatic constituents from the heated kerogen (Yang et al., 2009).

The surface properties change with the maturity of kerogen increasing. N_2-SSA of the kerogen samples decreases from 7.3 m^2/g for JR0 to 3.6 m^2/g for JR2 and then increases to 10.0 m^2/g for JR5 (Table 1, Fig. 2A). Thereafter, a sharp increase in N_2 SSA occurs in JR6 (27.5 m^2/g). This change pattern is consistent with the prior report (Yang et al., 2009). Under the initial thermal treatment, aliphatic chains were expanded and converted to a fluidal state, resulting in shrinkage of internal pores (Yang et al., 2009). In the moderate phase of maturity, the cracking of aliphatic chain opened new pores on matrices (Pignatello, 2012). However, the considerable increase

Table 4
Freundlich parameters for sorption and desorption, and hysteresis index of benzene.

Sample	Sorption				Desorption				Hysteresis index (HI)[a]
	logK_F[b]	n	R^2	N	logK_F	n	R^2	N	
RJ0	2.046(0.025)[c]	0.572(0.019)	0.99	12	2.247(0.010)	0.289(0.007)	0.99	12	0.51
RJ1	2.000(0.035)	0.588(0.026)	0.98	12	2.251(0.014)	0.274(0.011)	0.98	12	0.47
RJ2	2.068(0.021)	0.460(0.016)	0.99	12	2.295(0.007)	0.239(0.005)	0.99	12	0.52
RJ3	2.086(0.031)	0.571(0.023)	0.98	12	2.343(0.011)	0.275(0.008)	0.99	12	0.48
RJ4	2.097(0.014)	0.389(0.010)	0.99	12	2.329(0.003)	0.264(0.002)	1.00	12	0.68
RJ5	2.112(0.007)	0.299(0.006)	1.00	12	2.211(0.007)	0.204(0.005)	0.99	12	0.68
RJ6	1.861(0.010)	0.289(0.007)	0.99	12	1.979(0.024)	0.209(0.018)	0.93	12	0.72

[a] The calculation of HI is detailed in Sun et al. (2013) ($HI = n_{desorption}/n_{sorption}$).
[b] The unit of K_F is μL/g.
[c] Standard deviation.

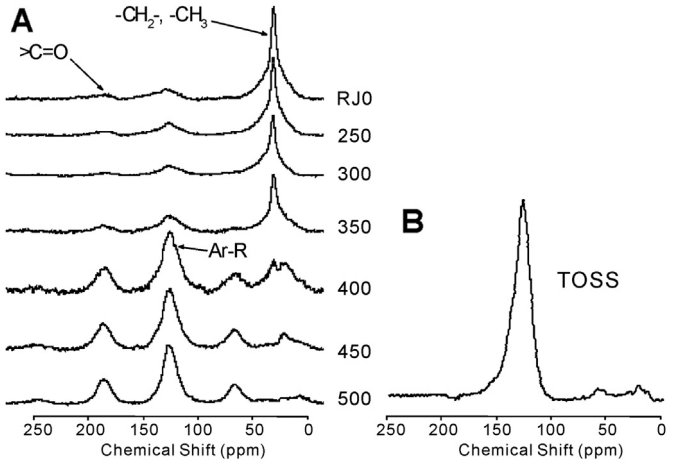

Fig. 1. Cross-polarization/magic angle spinning (CP/MAS) ^{13}C nuclear magnetic resonance (^{13}C NMR) spectra (A) for the kerogen samples, and a TOSS spectrum (B) for the most matured kerogen (500 °C).

in N_2-SSA for RJ6 seems to be not in accordance with the porous changes during maturation (Durand, 1980). As aliphatic C between the graphitic interlayers was extensively removed at high maturity phase, the interlayers became closer. This would cause a decrease in the amount of micropores (Durand, 1980). The above phenomenon is likely due to the limitation of porosity characterization using N_2. Ran et al. (2007, 2013) found that N_2-SSA primarily reflected the surface area of mineral constituents, rather than internal porosity of organic matrices. This observation is further supported by a significant correlation between the ash contents and N_2-SSA for the lowly-matured kerogen samples (<450 °C) in the present study (Fig. 2B). Such correlation was also observed for some hydrothermal and thermal biochars (Sun et al., 2011). In contrast to N_2-SSA, the modeling microporosity based on the benzene sorption indicates a significant decrease in micropores in the most matured kerogen (see discussion later), which is consistent with the structural alteration.

3.2. Sorption behaviors of phenanthrene and benzene

The sorption isotherms of phenanthrene and benzene can be well fitted ($R^2 > 0.94$ for phenanthrene; $R^2 > 0.98$ for benzene) by the Freundlich model (Tables 3 and 4; Supplementary Data, Fig. S2). The sorption isotherms are nonlinear ($n = 0.40–0.78$ for phenanthrene; $n = 0.29–0.59$ for benzene). The nonlinearity of phenanthrene generally increases from JR0 ($n = 0.77$) to JR6 ($n = 0.40$), while that of benzene also increases as the n values change from 0.57 to 0.29 (Tables 3 and 4). In addition, the n values of the isotherms for phenanthrene and benzene are significantly correlated with the ratios of H/C ($r > 0.87$, $p < 0.05$) and O/C ($r > 0.83$, $p < 0.05$), the contents of aromatic and aliphatic C ($r > 0.87$, $p < 0.05$) and the vitrinite reflectance ($r > 0.92$, $p < 0.01$; Supplementary Data, Fig. S3). The increase in the nonlinearity with the kerogen maturation is probably associated with the exposure of rigid aromatic C and condensation of kerogen. Aromatic C had been considered as an important adsorption domain and was observed to be positively correlated to nonlinearity (Wen et al., 2007; Xing and Pignatello, 1997; Zhang et al., 2013). Zhu and Pignatello (2005) also attributed the nonlinearity of phenanthrene sorption to nanovoids within the rigid aromatic phases. The decreases in H/C, O/C, and aliphatic C content, as well as the increase in aromatic C content, indicate that the aromatic C percentage in the kerogen samples increases during thermal maturation. And the decrease in R_o suggests that the kerogen becomes more rigid during thermal maturation.

The K_{OC} values indicate the sorption affinity of the kerogen samples. The K_{OC} of phenanthrene increases from RJ0 to RJ5 and significantly decreases on RJ6 at different concentrations (Table 3). Such patterns also are observed for the benzene sorption on the original and matured kerogen, as evidenced by the log K_F (Table 4). This trend is associated with the chemical and porous changes of the kerogen during the thermal maturation. In the primary phase of maturation, the decarboxylation could elevate the hydrophobicity of kerogen, which is beneficial to the sorption of hydrophobic phenanthrene and benzene (Zhang et al., 2013). Thereafter, the cracking of aliphatic constitutes exposes rigid aromatic domain and generates micropores in the kerogen leading to the increases in the sorption of phenanthrene and benzene. But when the thermal maturation continued to increase, chemistry and structure of the highly matured kerogen significantly changed. Non-aromatic groups were almost eliminated, and aromatic interlayer became shrunk (Durand, 1980). The shrinkage between aromatic sheets could block the access of phenanthrene and benzene to internal micropores of the kerogen, leading to the considerable decrease in micropore volume at high maturation stage.

The sorption behaviors of phenanthrene and benzene on the kerogen samples are very similar to each other, as evidenced by significant correlations of their $V_{o,d}$ and n values (Fig. 3A–B). This indicates a similar mechanism for their sorption on the kerogen samples. The significant correlations of their $V_{o,d}$ also reflect that the microporosity characterized by the gaseous benzene sorption effectively explains the sorption behavior of phenanthrene on the kerogen samples. As discussed above, chemical functionality, microporosity, and structure of the kerogen control the sorption behaviors of phenanthrene and benzene. These factors are also important for the sorption of HOCs on biochars (Chun et al., 2004; Sun et al., 2011). A dominance of microspore-filling was observed for benzene sorption on a series of crop-derived chars, which had

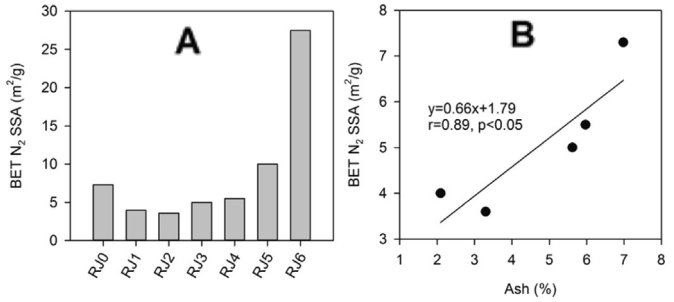

Fig. 2. N_2-specific surface area (SSA) of the kerogen samples (A) and their correlation (B) with ash content (wt%).

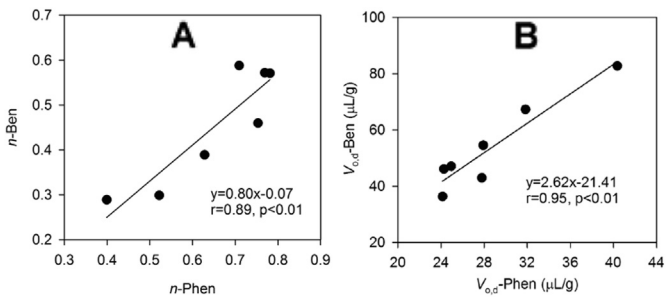

Fig. 3. Correlations between n (A) and $V_{o,d}$ (B) for the benzene and phenanthrene sorption on the kerogen samples.

relatively high surface affinity and areas (Chun et al., 2004). Besides, the acidity and basicity associated with oxygen-containing components also influenced the adsorption of benzene on the chars. Sun et al. (2011) found that aromatic C contents of thermally treated chars influenced nonlinearity but not necessarily the sorption capacity. The sorption capacity of the chars may be partly ascribed to aliphatic constituents.

The sorption isotherms of benzene on the kerogen samples are more nonlinear than those of phenanthrene (Tables 3 and 4), due in part to sorption competition between H_2O and phenanthrene in aquatic environment. Some high energy sites of sorbents could be occupied by H_2O molecular, resulting in decrease in the adsorption of phenanthrene (Kwon and Pignatello, 2005). It has been observed that the pore-filling process of HOCs by soil minerals can be suppressed by water (e.g. Chiou et al., 1988).

3.3. Desorption hysteresis of benzene

The desorption isotherms of benzene on the kerogen samples are nonlinear (Table 4; Supplementary Data, Fig. S4). And the nonlinearity for the desorption isotherms of benzene are higher than for the corresponding sorption isotherms. The desorption hysteresis indices (HI) ($n_{desorption}/n_{sorption}$) for benzene are presented in Table 4. As HI is smaller, the desorption hysteresis is larger. It is observed that different degrees of desorption hysteresis are present for all the kerogen samples (Table 4). Hysteresis indices (HI) increase from 0.51 for RJ0 to 0.72 for RJ6.

The highly matured kerogen shows stronger nonlinearity of desorption and higher HI values than the lowly matured kerogen. This phenomenon is likely associated with the pore deformation for the differently matured kerogen samples and the entrapment of benzene in the NOM matrix. The highly matured kerogen is condensed and rigid, and should be hardly expanded by benzene (Huang and Weber, 1997; Sun et al., 2013). In contrast, sorbed benzene may expand or penetrate the lowly matured kerogen at high concentrations, resulting in some tenant pores in the matrices (Braida et al., 2003). Braida et al. (2003) observed a pronounced volume swelling (two times) of a charcoal after benzene uptake. Moreover, the entrapment of benzene in NOM nanopore and aromatic graphitic interlayers is likely responsible for the observed hysteresis of benzene in the highly matured kerogen. Previous investigation demonstrated that aromatic NOCs can form the specific π–π bonds with the aromatic rings of the condensed NOM (Zhu and Pignatello, 2005). Huang and Weber (1997) observed that the desorption hysteresis of Phen was closely associated with the aromatic C of the peat, shale, and kerogen samples.

3.4. Importance of micropore-filling to sorption

The micropores-filling by different types of NOM contributes considerably to total sorption of HOCs (Ran et al., 2013). Here we estimated respectively the micropore sorption volumes ($V_{o,d}$) of benzene and phenanthrene on the kerogen samples using the DR model. The $V_{o,d}$ values are normalized to TOC of the kerogen samples and are illustrated in Fig. 4. The $V_{o,d}$ values of benzene generally increase from RJ0 to RJ5, and greatly decrease on RJ6. Such trend is also observed for phenanthrene, indicating that microporosity of the kerogen samples can be well characterized using gaseous benzene. The changes in microporosity are in accordance with those of the structures and sorption capacities for the differently matured kerogen, as demonstrated in the above sections.

The $V_{o,d}$ values of benzene on the kerogen samples are significantly related to, but constantly higher than those of phenanthrene, which could be explained by the effect of molecular sieve.

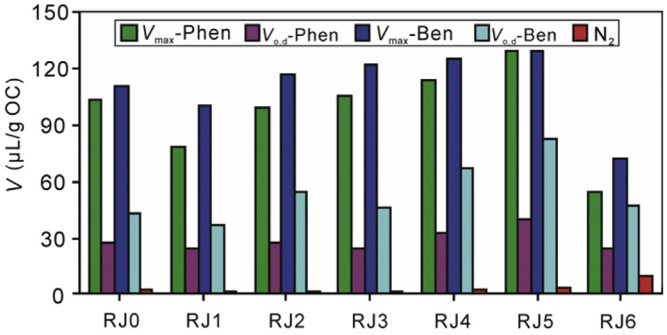

Fig. 4. Maximum sorption volumes and micropore volumes of phenanthrene and benzene, and N_2 adsorption volumes of the kerogen samples.

Apparently, some of relatively small micropores are available for the filling of small-sized benzene (0.341 nm × 0.666 nm × 0.729 nm), rather than for that of large-sized phenanthrene (0.341 nm × 0.999 nm × 1.094 nm). It can be expected that the pore-filling contribution is higher for the sorption of small molecular size HOCs than for that of large molecular size HOCs. The molecular sieving mechanism has been also observed for the sorption of dichlorobenzene, naphthalene, and trichlorobenzene by an aquifer kerogen (Ran et al., 2004). Ran et al. (2007) reported that the volume of the micropores of <0.7 nm could account for 58–73% of total micropore volume (0–1.4 nm) of a kerogen sample. Moreover, as the kerogen maturation increases, the variation of the $V_{o,d}$ values is larger for benzene than for phenanthrene, indicating that a fraction of the maturation-generated micropores of kerogen is relatively small in size.

The maximum sorption volumes V_{max} of benzene (53–130 μL/g) on the kerogen samples are very close to those of phenanthrene (71–129 μL/g; Fig. 4). Moreover, the V_{max} of benzene or phenanthrene is considerably higher than the sorption volume based on the N_2-SSA. This indicates that N_2-SSA could not be a suitable parameter reflecting the sorption capacity of NOM, especially for those containing plenty of internal micropores. Assuming that N_2-SSA primarily reflects the external pores of the kerogen samples (Ran et al., 2013), the adsorption on the surface of kerogen only accounts for 1.07–13.6% of the total sorption for benzene and phenanthrene (Fig. 4).

A comparison between the V_{max} and $V_{o,d}$ shows that the $V_{o,d}$ of phenanthrene on the kerogen samples accounts for 23–46% of the V_{max}, and that of benzene for 36–65%. This indicates that the micropore-filling process is a significant mechanism for the sorption of benzene and phenanthrene on the kerogen samples.

4. Conclusions

The sorption of benzene by the differently matured kerogen samples well reflects their microporosity, which is consistent with the structural changes of kerogen during maturation. As the maturation degree of the kerogen increases, the sorption volumes for phenanthrene increases initially and then decreases. Such pattern is also observed for the micropore adsorption volumes of gaseous benzene. The micropore volumes of benzene on the kerogen samples are significantly correlated with, but higher than those of phenanthrene, which is satisfactorily explained by the molecular sieve effect during the hole-filling process. Hysteresis occurs in the desorption of benzene on the kerogen samples, and is higher for the high matured kerogen than for the lower matured kerogen. This is probably associated with the pore deformation of NOM and entrapment of benzene in the NOM matrix. The micropore-filling volumes of phenanthrene and benzene on the

kerogen samples account for 23–46% and 36–65% of the maximum sorption volumes, respectively, indicating the importance of micropore-filling mechanism to the sorption of hydrophobic organic compounds.

Acknowledgment

We thank Dr. Baoshan Xing for the measurement of TOSS/CP ^{13}C NMR spectroscopy for the sample RJ06. This study was supported by a key project of NNSFC-Guangdong (U1201235), a "Team Project" and a general project of National Natural Science Foundation of China (41121063 and 41073082), and a Key Field Project, Chinese Academy of Sciences (Y234081A07). This is contribution No. IS-1766 from GIGCAS.

Appendix A. Supplementary data

Supplementary data related to this article can be found at http://dx.doi.org/10.1016/j.envpol.2013.10.039.

References

Braida, W.J., Pignatello, J.J., Lu, Y., Ravikovitch, P.I., Neimark, A.V., Xing, B., 2003. Sorption hysteresis of benzene in charcoal particles. Environ. Sci. Technol. 37, 409–417.
Chefetz, B., Xing, B., 2009. Relative role of aliphatic and aromatic moieties as sorption domains for organic compounds: a review. Environ. Sci. Technol. 43, 1680–1688.
Chiou, C.T., Kile, D.E., Malcolm, R.L., 1988. Sorption of vapors of some organic liquids on soil humic acid and its relation to partitioning of organic compounds in soil organic matter. Environ. Sci. Technol. 22, 298–303.
Chun, Y., Sheng, G., Chiou, C.T., Xing, B., 2004. Compositions and sorptive properties of crop residue-derived chars. Environ. Sci. Technol. 38, 4649–4655.
Corley, T.L., Farrell, J., Hong, B., Conklin, M.H., 1996. VOC accumulation and pore filling in unsaturated porous media. Environ. Sci. Technol. 30, 2884–2891.
Cornelissen, G., Gustafsson, Ö., Bucheli, T.D., Jonker, M.T.O., Koelmans, A.A., van Noort, P.C.M., 2005. Extensive sorption of organic compounds to black carbon, coal, and kerogen in sediments and soils: mechanisms and consequences for distribution, bioaccumulation, and biodegradation. Environ. Sci. Technol. 39, 6881–6895.
De Jonge, H., Mittelmeijer-Hazeleger, M.C., 1996. Adsorption of CO_2 and N_2 on soil organic matter: nature of porosity, surface area, and diffusion mechanisms. Environ. Sci. Technol. 30, 408–413.
Durand, B., 1980. Kerogen: Insoluble Organic Matter from Sedimentary Rocks. Editions technip, Paris, France.
Gan, H., Nandi, S., Walker Jr., P., 1972. Nature of the porosity in American coals. Fuel 51, 272–277.
Huang, W., Weber, W.J., 1997. A distributed reactivity model for sorption by soils and sediments. 10. Relationships between desorption, hysteresis, and the chemical characteristics of organic domains. Environ. Sci. Technol. 31, 2562–2569.
Kleineidam, S., Schüth, C., Grathwohl, P., 2002. Solubility-normalized combined adsorption-partitioning sorption isotherms for organic pollutants. Environ. Sci. Technol. 36, 4689–4697.
Kwon, S., Pignatello, J.J., 2005. Effect of natural organic substances on the surface and adsorptive properties of environmental black carbon (char): pseudo pore blockage by model lipid components and its implications for N_2-probed surface properties of natural sorbents. Environ. Sci. Technol. 39, 7932–7939.
Larsen, J.W., Hall, P., Wernett, P.C., 1995. Pore structure of theArgonne premium coals. Energy Fuels 9, 324–330.
Li, J., Werth, C.J., 2001. Evaluating competitive sorption mechanisms of volatile organic compounds in soils and sediments using polymers and zeolites. Environ. Sci. Technol. 35, 568–574.
Luthy, R.G., Aiken, G.R., Brusseau, M.L., Cunningham, S.D., Gschwend, P.M., Pignatello, J.J., Reinhard, M., Traina, S.J., Weber, W.J., Westall, J.C., 1997. Sequestration of hydrophobic organic contaminants by geosorbents. Environ. Sci. Technol. 31, 3341–3347.
Pignatello, J.J., 2012. Dynamic interactions of natural organic matter and organic compounds. J. Soils Sediments 12, 1241–1256.
Pignatello, J.J., Xing, B., 1996. Mechanisms of slow sorption of organic chemicals to natural particles. Environ. Sci. Technol. 30, 1–11.
Ran, Y., Huang, W., Rao, P., Liu, D., Sheng, G., Fu, J., 2002. The role of condensed organic matter in the nonlinear sorption of hydrophobic organic contaminants by a peat and sediments. J. Environ. Qual. 31, 1953–1962.
Ran, Y., Sun, K., Yang, Y., Xing, B., Zeng, E., 2007. Strong sorption of phenanthrene by condensed organic matter in soils and sediments. Environ. Sci. Technol. 41, 3952–3958.
Ran, Y., Xiao, B., Huang, W., Peng, P.A., Liu, D., Fu, J., Sheng, G., 2003. Kerogen in aquifer material and its strong sorption for nonionic organic pollutants. J. Environ. Qual. 32, 1701–1709.
Ran, Y., Xing, B., Rao, P.S.C., Fu, J., 2004. Importance of adsorption (hole-filling) mechanism for hydrophobic organic contaminants on an aquifer kerogen isolate. Environ. Sci. Technol. 38, 4340–4348.
Ran, Y., Yang, Y., Xing, B., Pignatello, J.J., Kwon, S., Su, W., Zhou, L., 2013. Evidence of micropore filling for sorption of nonpolar organic contaminants by condensed organic matter. J. Environ. Qual. 42, 806–814.
Ravikovitch, P.I., Bogan, B.W., Neimark, A.V., 2005. Nitrogen and carbon dioxide adsorption by soils. Environ. Sci. Technol. 39, 4990–4995.
Sun, K., Ran, Y., Yang, Y., Xing, B., Mao, J., 2013. Interaction mechanism of benzene and phenanthrene in condensed organic matter: importance of adsorption (nanopore-filling). Geoderma 204, 68–74.
Sun, K., Ro, K., Guo, M., Novak, J., Mashayekhi, H., Xing, B., 2011. Sorption of bisphenol A, 17α-ethinyl estradiol and phenanthrene on thermally and hydrothermally produced biochars. Bioresour. Technol. 102, 5757–5763.
Weber, W.J., Huang, W., 1996. A distributed reactivity model for sorption by soils and sediments. 4. Intraparticle heterogeneity and phase-distribution relationships under nonequilibrium conditions. Environ. Sci. Technol. 30, 881–888.
Weber, W.J., Young, T.M., 1997. A distributed reactivity model for sorption by soils and sediments. 6. Mechanistic implications of desorption under supercritical fluid conditions. Environ. Sci. Technol. 31, 1686–1691.
Wen, B., Zhang, J.-j., Zhang, S.-z., Shan, X.-q., Khan, S.U., Xing, B., 2007. Phenanthrene sorption to soil humic acid and different humin fractions. Environ. Sci. Technol. 41, 3165–3171.
Xing, B., Pignatello, J.J., 1997. Dual-mode sorption of low-polarity compounds in glassy poly (vinyl chloride) and soil organic matter. Environ. Sci. Technol. 31, 792–799.
Xing, B., Pignatello, J.J., Gigliotti, B., 1996. Competitive sorption between atrazine and other organic compounds in soils and model sorbents. Environ. Sci. Technol. 30, 2432–2440.
Yang, C., Huang, W., Fu, J., Dang, Z., 2009. Impact of kerogen heterogeneity on sorption of organic pollutants. 1. Sorbent characterization. Environ. Toxicol. Chem. 28, 1585–1591.
Zhang, Y., Ran, Y., Mao, J., 2013. Role of extractable and residual organic matter fractions on sorption of phenanthrene in sediments. Chemosphere 90, 1973–1979.
Zhu, D., Pignatello, J.J., 2005. Characterization of aromatic compound sorptive interactions with black carbon (charcoal) assisted by graphite as a model. Environ. Sci. Technol. 39, 2033–2041.